Measuring 3-D Location and Shape Parameters of Cylinders by a Spatial Encoding Technique

Zen Chen, Tsorng-Lin Chia, and Shinn-Ying Ho

Abstract—We are concerned with the problem of estimation of true cylinder radius, height, location, and orientation. We present mathematical models for measuring these location and shape parameters using a spatial encoding technique. A crucial step in the proposed method is to convert the estimation problem with complex curved stripe patterns to an equivalent, but simpler, estimation problem with line stripe patterns. The notions of silhouette edges and virtual plane are introduced. Various projective geometry techniques are applied to derive the cylinder location and shape parameters. The actual experiment apparatus is set up to employ the developed mathematical models to measure the cylinder geometric parameters. Description of the image-processing tasks for extracting perceived curved stripes and stripe endpoints is given. Sensitivity analysis and proper measures are taken to consider the effects of the uncertainties of stripe endpoints and silhouette edge locations on the measurement. Experiments have confirmed that our measurement method yields quite good results for different cylinders under various measurement environment conditions.

I. INTRODUCTION

IN THE LITERATURE, the estimation of the cylindrical surface parameters related to the cylinder radius, location, and orientation is often done by surface fitting of points on the surface [1]–[3] or curve fitting of elliptical curves marked on the surface [4]–[8]. The mathematical models for these two approaches are briefly reviewed here in order to point out the difficulties they face. A number of coordinate systems will be first introduced for the surface measurement. Let an object-centered coordinate system be attached to the cylinder in which a reference point on the cylinder axis is defined as the origin, the cylinder axis is chosen to be the Z_0 axis, and the X_0 and Y_0 axes are selected such that they form, together with the Z_0 axis, the three principal coordinate axes of the system. The second coordinate system, called the viewer (or camera) coordinate system (X_v, Y_v, Z_v), is a rectangular coordinate system located at a certain location with a particular orientation with respect to the object-centered system. The third coordinate system, called the image coordinate system (X_I, Y_I, Z_I), is defined with respect to the viewer coordinate system whose origin is located at $(0, 0, f)$ on the Z_v axis, while the Z_I axis is parallel to the Z_v axis, and the X_I-Y_I plane is parallel to the X_v-Y_v plane, but not necessarily in the same orientation.
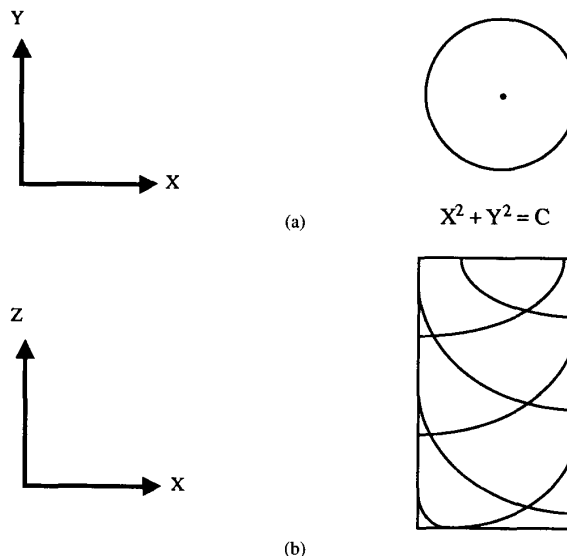
Fig. 1. The top and side views of a cylinder used in a surface fitting process. (a) Top view. (b) Side view.

In Fig. 1 the top and side views of a cylinder are shown. In the object-centered coordinate system let $P_i = (X_{oi}, Y_{oi}, Z_{oi}), i = 1, 2, \cdots, n$, be the points on the cylinder surface, then they are given by $X_{oi}^2 + Y_{oi}^2 = R^2$. In the viewer coordinate system, these points are transformed to $P_i = (X_{vi}, Y_{vi}, Z_{vi})$ and the circular contour becomes

$$AX_{vi}^2 + BY_{vi}^2 + CZ_{vi}^2 + DX_{vi}Y_{vi} + EX_{vi}Z_{vi} + FY_{vi}Z_{vi} + G = 0 \tag{1}$$

where the coefficients A, B, C, D, E, F, and G are derived from the coordinate transformation matrix between the two involved coordinate systems. The coefficients of linear terms become null when the viewer coordinate system origin is on the cylinder axis. These coefficients have to be estimated in order to measure the cylinder location and shape parameters. One popular way to get 3-D points on the object surface (in the viewer coordinate system) is via triangulation techniques [9]–[12]. However, these methods are noise-sensitive and need to solve the point correspondence problem [13], [14].

On the other hand, in the curve-fitting approach, a set of elliptical curves is usually created on the cylindrical surface by casting parallel sheets of light on the object surface under a parallel projection assumption, as shown in Fig. 1(b). Again, let $P_i = (X_{oi}, Y_{oi}, Z_{oi}), i = 1, 2, \cdots, n$ be n points of a
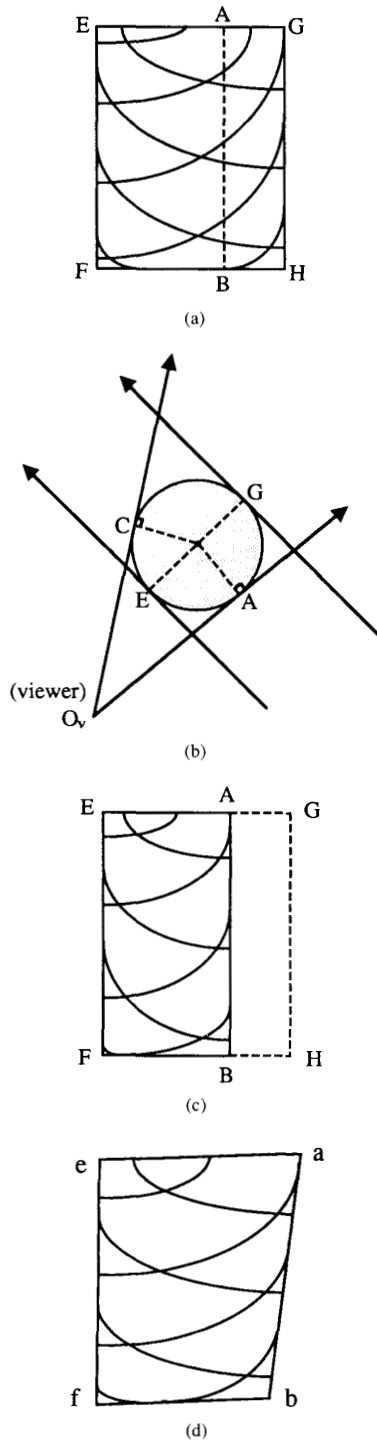
Fig. 2. The stripe patterns, silhouette edges, and the viewing geometry.

Fig. 3. The imaged virtual plane and line stripes pattern used in an equivalent estimation problem.

particular elliptical curve on the cylindrical surface. In the object-centered and viewer coordinate systems the n points are characterized by the same family of mathematical equations given in (1).
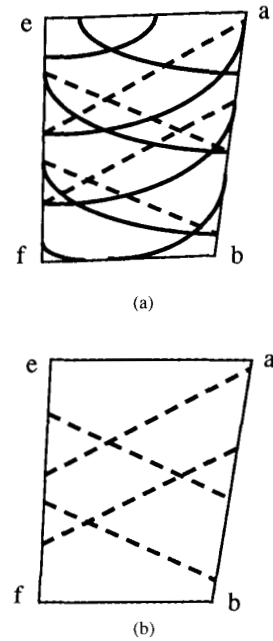
Thus, in these two approaches, the form of the cylindrical surface is governed by a quadric equation containing six coefficients. This representation is further complicated by a nonlinear perspective projection that is performed in order to derive the image coordinates of surface points or surface curves on the image plane. Since the imaging process is characterized by a nonlinear perspective projection, quite often some assumptions are made to approximate this projection by a parallel projection [15]–[19]. A faithful mathematical modeling of the cylinder measurement from the imaged data is quite complex, and therefore the estimation is very hard, if not impossible. With this observation in mind, we shall look for a different approach that is simple and effective.

Our proposed method is a spatial encoding technique [16]–[23] using two orthogonal sets of grid patterns. This technique was originally proposed in [15], [16] to extract surfaces with different orientations. Later on, similar techniques were used by many authors to derive the surface orientation, structure, relative depth, etc. [17]–[19]. In these methods the imaging process is approximated by a parallel projection to avoid the nonlinear process of a perspective projection. As a result of this approximation, no absolute size or depth of the object is possible to compute. In this study we shall deal with the absolute size, height, location, and orientation of the cylinder. First of all, the cylinder estimation problem with the complex curved stripe pattern is properly transformed to an equivalent, but simpler, one with a line stripe pattern. This is done through the introduction of a virtual plane defined by two silhouette edges on the cylinder. For measuring the cylinder location and shape parameters, proper mathematical models for individual measurements are developed. The whole measurement principle will be
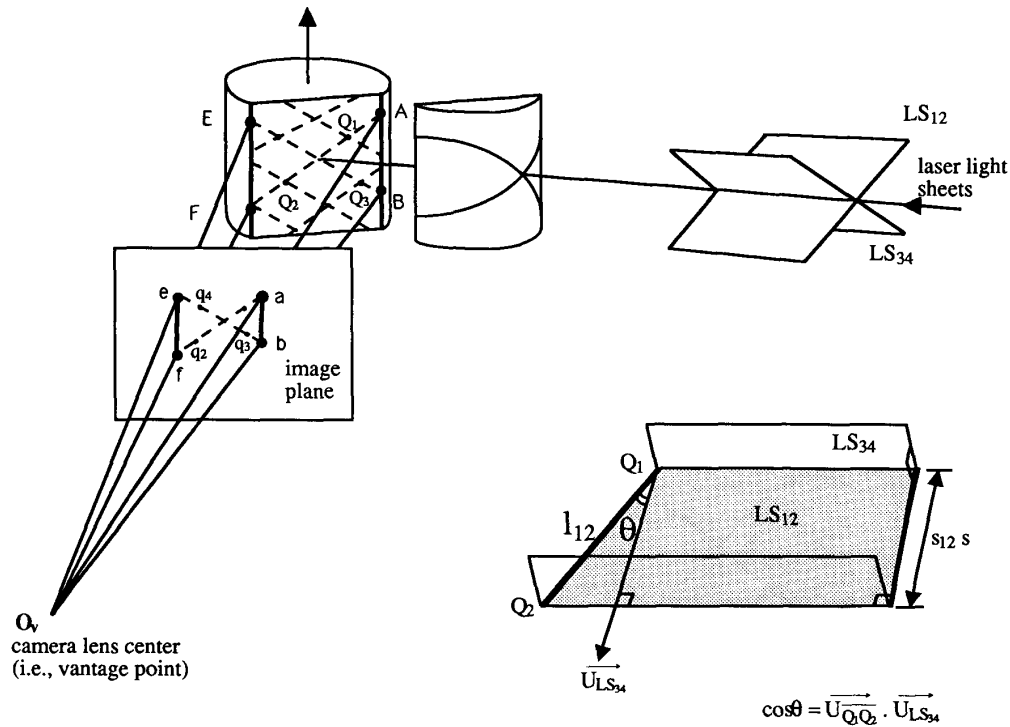
Fig. 4. The viewing geometry and imaging process of the stripe pattern on the virtual plane created by laser light sheets.

examined by experiments. The experiment apparatus and image processing techniques used to extract the perceived curved stripes and stripe endpoints are described. Experiments are conducted under various measurement environment conditions for three different cylinders. Sensitivity analysis and proper measures are taken to consider the effects of uncertainties of stripe endpoints and silhouette edge locations on the measurement.

In the rest of the paper, Section II describes the formation of visible silhouette edges that delimit a visible surface patch marked with crossing stripes. More importantly, we define a virtual plane and convert a complicated curved stripe estimation problem to an equivalent, but simpler, estimation problem with line stripes. Section III presents the step-by-step estimation of the cylinder axis. Section IV gives the estimation method for the cylinder axis location and the cylinder radius. Section V covers the estimation of the cylinder height. In Section VI experiment results and sensitivity analysis are reported. Section VII contains a conclusion.

II. FORMATION OF SILHOUETTE EDGES AND VIRTUAL PLANE

In this method, two sets of grid patterns are generated, for example, with an expanded laser beam cast through a grid plane with equal spacings in the two orthogonal X and Y directions [24]. The X and Y light sheets travel in space along a direction perpendicular to the X and Y sheets. When they are blocked by a cylinder, two sets of elliptical stripes on the

cylindrical surface are created and imaged on the X_I-Y_I image plane. The stripe pattern is shown in Fig. 2(a). Lines $\overline{EF}$ and $\overline{GH}$ are defined by the stripe endpoints created by the X and Y light sheets and they can be easily shown to be two tangent lines on the cylindrical surface. They are called hereafter the silhouette edges of the cylinder.

On the other hand, in the viewer coordinate system the visible part of the cylindrical surface is determined by the field of view at the vantage point. In the case where the viewer is an imaging camera, the vantage point is the lens center. Assume the cylinder is completely within the field of view (this is generally the case if the object is not too close to the viewer). From the optical geometry shown in Fig. 2(b), the extent of the object surface visible to the viewer (camera) is represented by the angle subtended by the chord $\overline{AC}$. It can be shown that the ray from the vantage point O_v to point C, $\overline{O_vC}$, is perpendicular to a radius of the circle, that is a cross section view, passing through point C. Similarly, the ray $\overline{O_vA}$ is perpendicular to another radius passing through point A. Assume the portion of the visible cylindrical surface between the two silhouette edges $\overline{AB}$ and $\overline{CD}$ overlaps with the lighted portion between the silhouette edges $\overline{EF}$ and $\overline{GH}$ defined in Fig. 2(b). Then, the visible elliptical stripes on the cylindrical surface are obtained, as shown in Fig. 2(c). In the rest of the paper we shall be concerned with the surface patch bounded by silhouette edges $\overline{AB}$ and $\overline{EF}$ only. This surface patch is imaged on the image plane (i.e., the X_I-Y_I plane) under a perspective projection, as shown in Fig. 2(d). Notice that on
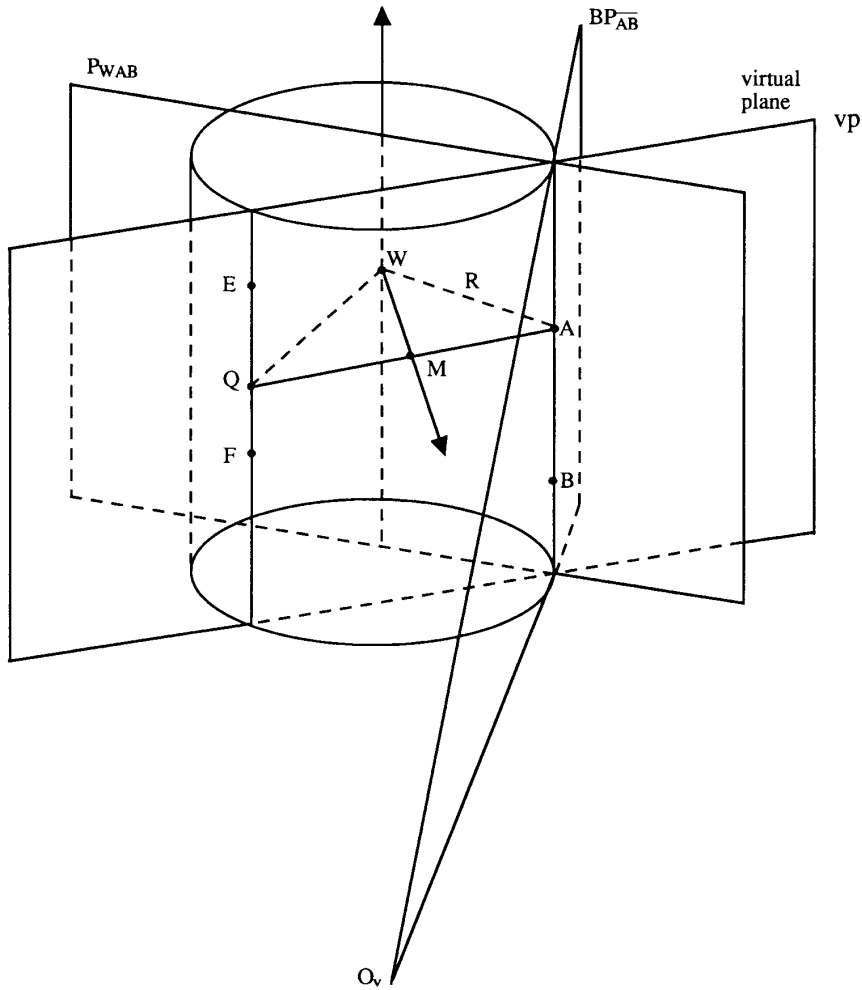
Fig. 5. The geometry for the estimation of cylinder axis location and cylinder radius.

the image plane the two perceived cylinder silhouette edges $\overline{ab}$ and $\overline{ef}$ becomes nonparallel due to the effect of the perspective transformation, when the image plane is not parallel to the cylinder axis. The elliptical stripes on the cylindrical surface after projection on the image plane are no longer elliptical, either.

Next, in Fig. 3(a) let us consider the dotted straight lines constructed between endpoint pairs of the elliptical stripes on the surface patch bounded by perceived silhouette edges $\overline{ab}$ and $\overline{ef}$. It is important to point out that these dotted straight lines are essentially the image of the line stripes that will be marked on the flatted surface virtually constructed between $\overline{AB}$ and $\overline{EF}$ by the original light sheets. We shall call the flatted surface a virtual plane. The original imaged curved stripe pattern in Fig. 3(a) is conceptually replaced by the line stripe pattern on the virtual plane, as shown in Fig. 3(b). So we shall convert the estimation problem related to the curved stripe image to an equivalent estimation problem based on the line stripe image. This is of vital importance to this research.

III. THE ESTIMATION OF CYLINDER AXIS DIRECTION

The cylinder axis direction can be estimated next. This axis direction is physically parallel to silhouette edges $\overline{AB}$ and $\overline{EF}$ on the cylindrical surface patch. Therefore, we shall estimate the line direction of $\overline{AB}$ and $\overline{EF}$ that is observable, rather than the cylinder axis itself, which is unobservable. To get the line direction of $\overline{AB}$ or $\overline{EF}$, we shall work with the virtual plane on which $\overline{AB}$ and $\overline{EF}$ are located.

A. The Plane Equation of the Virtual Plane

We shall modify the method developed previously in our laboratory [24] to estimate the plane equation for the virtual plane. Let the viewing geometry of the virtual plane and the line stripes on it be depicted in Fig. 4. In this figure let $\overline{Q_1Q_2}$ and $\overline{Q_3Q_4}$ be two sufficiently long line stripes with s_{12} and s_{34} grid units that are cast by two certain crossing light sheets LS_{12} and LS_{34}. Also let the images of these four points be $q_i, i = 1, 2, 3, 4$. The main steps for determining the 3-D
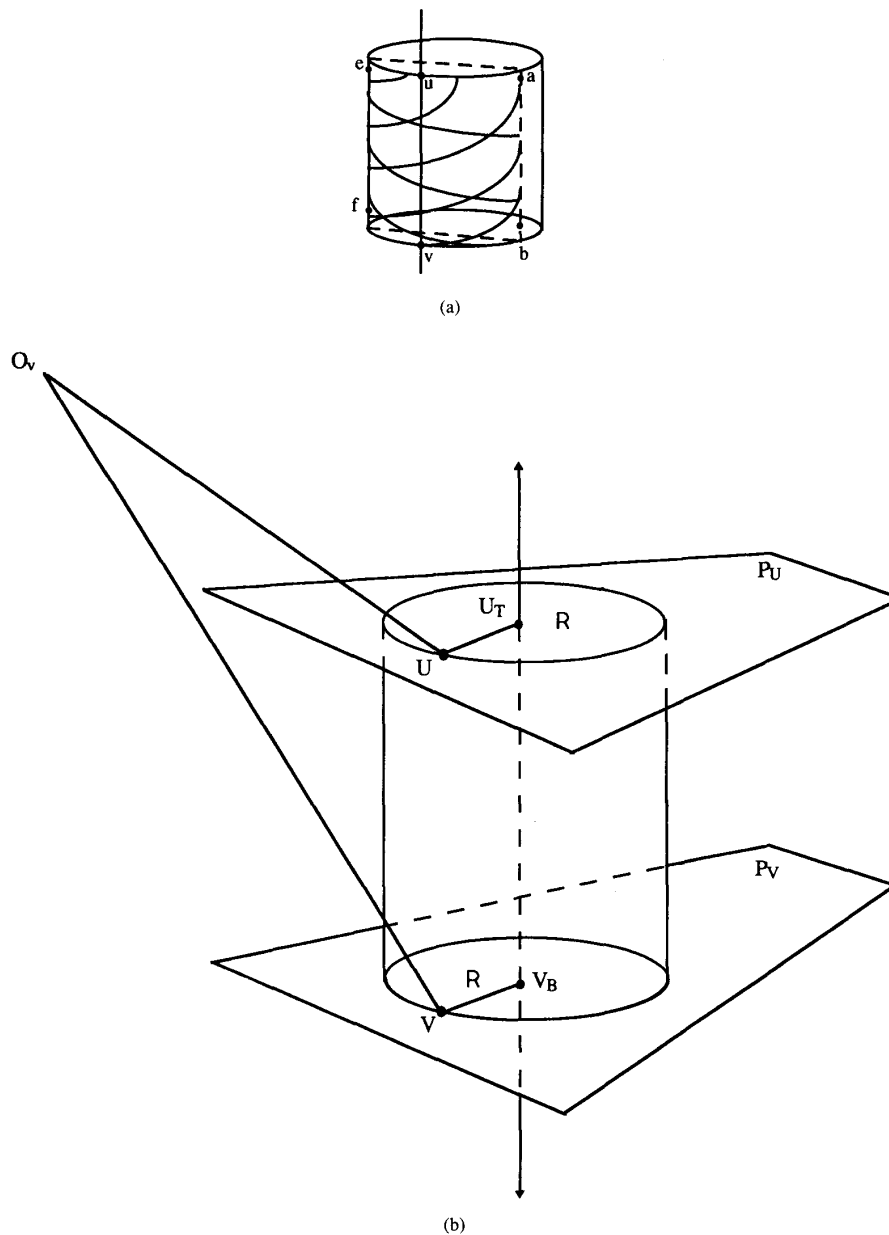
(a)

(b)

Fig. 6. The geometry for the estimation of cylinder height.

plane equation of the virtual plane defined on the cylinder are described as follows:

1) Through a calibration process the unit normal vectors of light sheets LS_{12} and LS_{34} can be determined as $\overrightarrow{U_{LS_{12}}}$ and $\overrightarrow{U_{LS_{34}}}$ with respect to the image coordinate system [24].

2) Let the vantage point O_V and the imaged line stripes $\overline{q_1 q_2}$ and $\overline{q_3 q_4}$ on the image plane define two backprojection planes $BP_{\overline{q_1 q_2}}$ and $BP_{\overline{q_3 q_4}}$. Let their unit normal vectors be given by $\overrightarrow{U_{BP_{\overline{q_1 q_2}}}}$ and $\overrightarrow{U_{BP_{\overline{q_3 q_4}}}}$.

3) Find the two cross products: $\overrightarrow{U_{LS_{12}}} \times \overrightarrow{U_{BP_{\overline{q_1 q_2}}}}$ and $\overrightarrow{U_{LS_{34}}} \times \overrightarrow{U_{BP_{\overline{q_3 q_4}}}}$. Let the unit vectors of these two cross-products be $\overrightarrow{U_{\overline{Q_1 Q_2}}}$ and $\overrightarrow{U_{\overline{Q_3 Q_4}}}$, then $\overrightarrow{U_{\overline{Q_1 Q_2}}}$ and $\overrightarrow{U_{\overline{Q_3 Q_4}}}$ are actually the line directions of line $\overline{Q_1 Q_2}$ and $\overline{Q_3 Q_4}$ on the virtual plane defined in Fig. 4.

4) The normal vector of the virtual plane is given by the cross product of $\overrightarrow{U_{\overline{Q_1 Q_2}}}$ and $\overrightarrow{U_{\overline{Q_3 Q_4}}}$. Let the unit vector of the cross product be denoted as $\overrightarrow{U_{VP}} = (a, b, c)$ or $(-a, -b, -c)$.
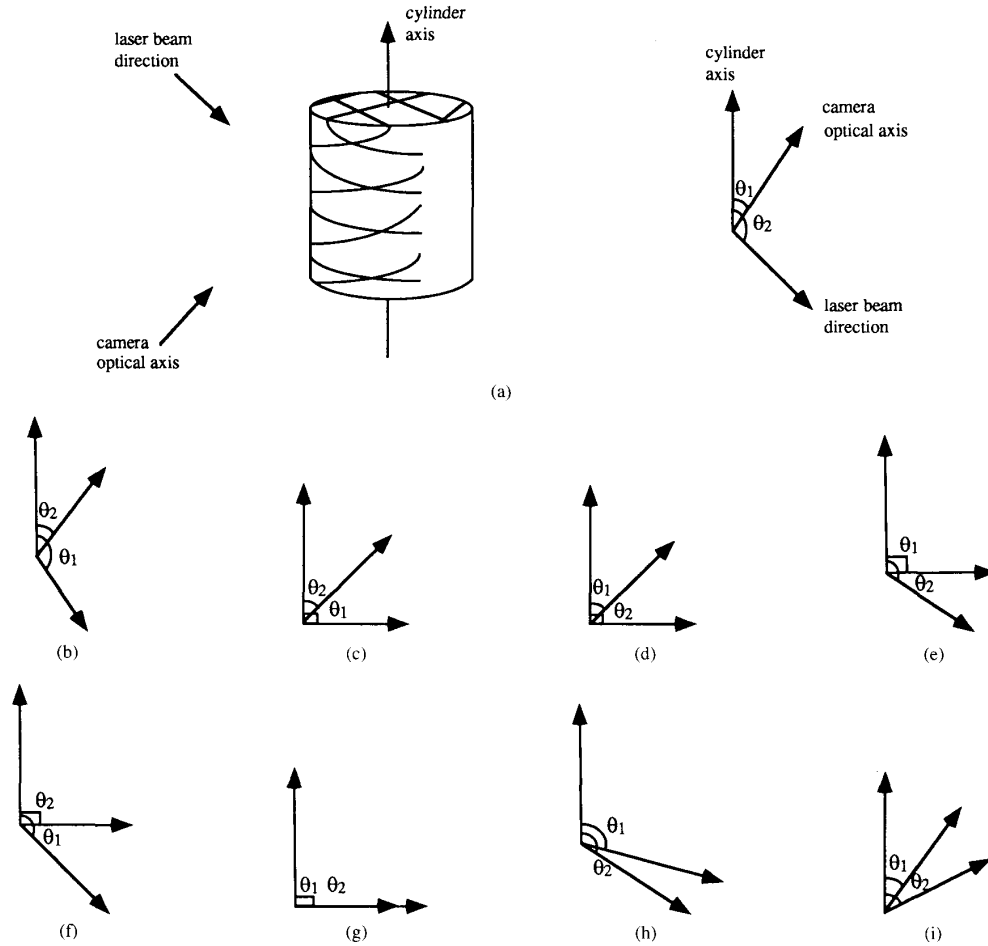
Fig. 7.   The selection rule used in the estimation procedure of cylinder height. (a), (b) $\cos\theta_1 \cdot \cos\theta_2 < 0$, (c), (d), (e), (f), (g) $\cos\theta_1 \cdot \cos\theta_2 = 0$, (h), (i) $\cos\theta_1 \cdot \cos\theta_2 > 0$.

5) The virtual plane equation can be represented by $aX_i + bY_i + cZ_i = d$ if $aX_i + bY_i + cZ_i \geq 0$, otherwise, $-aX_i - bY_i - cZ_i = d, i = 1, 2, 3, 4$, where d is the distance between the virtual plane and the vantage point. The value of d is determined below.

On the image plane the perspective projection of $Q_i = (X_i, Y_i, Z_i), i = 1, 2, 3, 4$, are specified, by

$$x_i = \frac{X_i f}{Z_i} \quad \text{and} \quad y_i = \frac{Y_i f}{Z_i}$$

where f is known (the focal length if a camera is used). Then d is given by a dot product:

$$d = \begin{cases} (a, b, c) \cdot (X_i, Y_i, Z_i), & \text{if } (a, b, c) \cdot (X_i, Y_i, Z_i) \geq 0 \\ -(a, b, c) \cdot (X_i, Y_i, Z_i), & \text{otherwise} \end{cases}$$
$$= \begin{cases} Z_i \left(\frac{ax_i}{f} + \frac{by_i}{f} + c \right), & \text{if } (a, b, c) \cdot (X_i, Y_i, Z_i) \geq 0 \\ -Z_i \left(\frac{ax_i}{f} + \frac{by_i}{f} + c \right), & \text{otherwise} \end{cases}$$
$$\equiv Z_i \alpha_i$$

Since the value of d is nonnegative, so the sign of α_i must be chosen to be identical with that of Z_i.

Thus,

$$(X_i, Y_i, Z_i) = \left(\frac{x_i}{\alpha_i f}, \frac{y_i}{\alpha_i f}, \frac{1}{\alpha_i} \right) d \tag{2}$$

Recall that line $\overline{Q_1 Q_2}$ on the virtual plane is cast by light sheet LS_{12} and the corresponding number of grid cells that are formed by the intersections of two sets of grid lines is s_{12}. Therefore, the length of line $\overline{Q_1 Q_2}$, denoted by l_{12}, is given by

$$l_{12} |\cos\theta| = l_{12} |(\overrightarrow{U_{Q_1 Q_2}} \cdot \overrightarrow{U_{\text{LS}_{34}}})| = s_{12} s \tag{3}$$

where s is the constant spacing between two adjacent X or Y light sheets and the pair of vertical bars denotes the absolute value. From (3) we can compute the value of l_{12}. From (2) l_{12} is also given by

$$l_{12} = d \left[\left(\frac{x_1}{\alpha_1 f} - \frac{x_2}{\alpha_2 f} \right)^2 + \left(\frac{y_1}{\alpha_1 f} - \frac{y_2}{\alpha_2 f} \right)^2 \right.$$
$$\left. + \left(\frac{1}{\alpha_1} - \frac{1}{\alpha_2} \right)^2 \right]^{1/2} \tag{4}$$
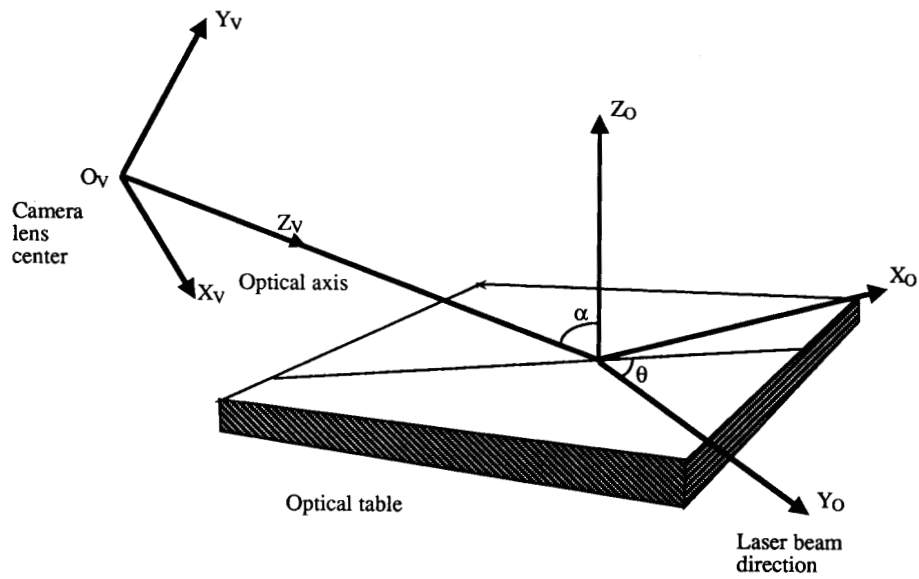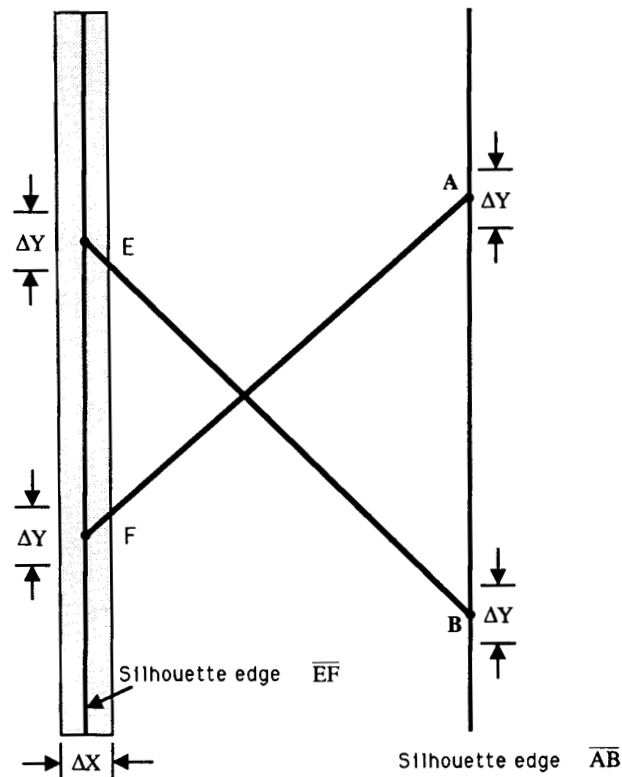
Fig. 8.   The geometry of the sensing environment.

Fig. 9.   An error model for stripe endpoint noise analysis.

From (3) and (4) we can solve for d. Thus we have completed the determination of the plane equation for the virtual plane.

B. The Cylinder Axis Direction

After the virtual plane is determined, we can proceed to find the location and shape parameters of the cylinder. Let us

TABLE I
MEASUREMENT RESULTS OF THE THREE CYLINDERS WITH THE CONFIGURATION PARAMETERS
$\alpha = 90°, \theta = 15°, 30°$, AND $45°$ AND THE CAMERA-TO-OBJECT DISTANCE IS ABOUT 900 MM

θ	est. value items object	C1 (35 mm, 125 mm)	C2 (35 mm, 80 mm)	C3 (15 mm, 80 mm)
15°	Radius	35.97	37.43	15.13
	R. error %	2.77	6.94	0.86
	Height	119.81	79.47	77.81
	H. error %	4.15	0.66	2.74
30°	Radius	32.87	33.68	14.31
	R. error %	6.08	3.77	4.60
	Height	129.74	82.22	82.71
	H. error %	3.79	2.78	3.38
45°	Radius	35.88	34.99	13.51
	R. error %	2.51	0.00	9.93
	Height	130.99	81.53	74.15
	H. error %	4.79	1.91	7.31

The average radius error % = 4.16%
The average height error % = 3.5%

consider the estimation of cylinder axis direction first. In Fig. (4), let silhouette edges $\overline{AB}$ and $\overline{EF}$ be imaged and the imaged silhouette edges be lines $\overline{ab}$ and $\overline{ef}$ on the image plane. Now the unit line directions of the two silhouette edges, $\overrightarrow{U_{\overline{AB}}}$ and $\overrightarrow{U_{\overline{EF}}}$ can be easily shown to be the cross products of the unit normal vectors of backprojection plane $BP_{\overline{AB}}$ and $BP_{\overline{EF}}$ with the unit normal vector of virtual plane $\overrightarrow{U_{VP}}$ derived previously. Namely,

$$\overrightarrow{U_{\overline{AB}}} = \overrightarrow{U_{BP_{\overline{AB}}}} \times \overrightarrow{U_{VP}}/|\overrightarrow{U_{BP_{\overline{AB}}}} \times \overrightarrow{U_{VP}}| \quad \text{and}$$

$$\overrightarrow{U_{\overline{EF}}} = \overrightarrow{U_{BP_{\overline{EF}}}} \times \overrightarrow{U_{VP}}/|\overrightarrow{U_{BP_{\overline{EF}}}} \times \overrightarrow{U_{VP}}|$$

where the unit normal vectors of backprojection planes $BP_{\overline{AB}}$ and $BP_{\overline{EF}}$ are given by

$$\overrightarrow{U_{BP_{\overline{AB}}}} = \overrightarrow{O_v a} \times \overrightarrow{O_v b}/|\overrightarrow{O_v a} \times \overrightarrow{O_v b}| \quad \text{and}$$

$$\overrightarrow{U_{BP_{\overline{EF}}}} = \overrightarrow{O_v e} \times \overrightarrow{O_v f}/|\overrightarrow{O_v e} \times \overrightarrow{O_v f}|.$$

Therefore the cylinder axis direction is given by either $\overrightarrow{U_{\overline{AB}}}$ or $\overrightarrow{U_{\overline{EF}}}$.

IV. THE ESTIMATION OF CYLINDER AXIS LOCATION AND CYLINDER RADIUS

Next, the cylinder axis location and cylinder radius can be estimated from the following step-by-step procedure (Please refer to Fig. 5):

A. Procedure for Estimation of Cylinder Axis Location and Cylinder Radius

1) Construct a plane, P_{WAB}, that contains the silhouette edge $\overline{AB}$ and is perpendicular to the backprojection plane $BP_{\overline{AB}}$ defined by $\overline{AB}$ and the vantage point. (Note that the backprojection plane is, by definition, a tangent plane of the cylinder.)
2) Construct a plane, P_{WAQ}, that contains point A and is perpendicular to the virtual plane. Let point Q be the intersection point between silhouette edge $\overline{EF}$ and plane P_{WAQ}.
3) Construct the bisection line, $\overline{MW}$, of line $\overline{AQ}$ on plane P_{WAQ} such that $\overline{MW}$ is perpendicular to $\overline{AQ}$ and M is the middle point of $\overline{AQ}$.
4) Find the intersection point, W, between line $\overline{MW}$ and plane P_{WAB}. Compute the distance between points W and A, denoted as $D_{\overline{WA}}$.

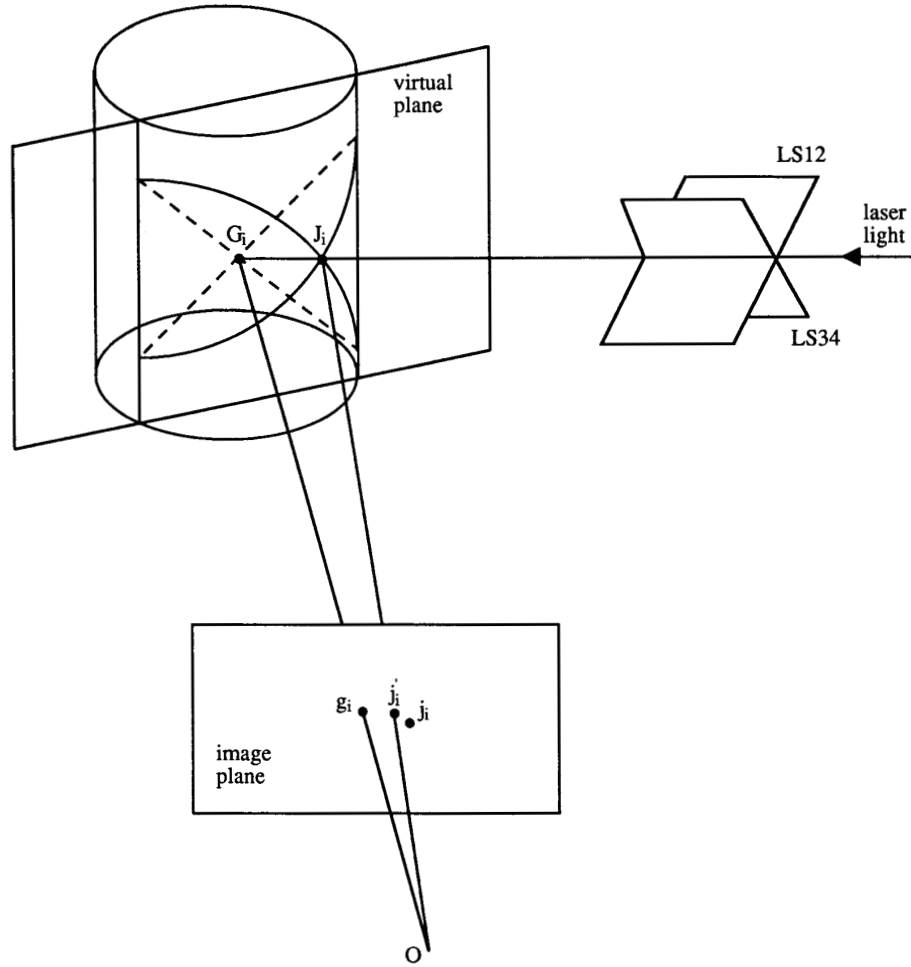*Theorem:* From the above estimation procedure, it can be shown

Fig. 10. The geometry for the iterative refinement.

1) point W is on the cylinder axis, and
2) $D_{\overline{WA}}$ is the cylinder radius.

Proof: The proof is rather straightforward. First, we must show that plane P_{WAB} contains the cylinder axis. Line $\overline{AB}$ is a silhouette edge and is tangent to the cylindrical surface. It follows immediately that backprojection plane $BP_{\overline{AB}}$ is a tangent plane to the cylindrical surface. Plane P_{WAB} is perpendicular to backprojection plane $BP_{\overline{AB}}$ and contains line $\overline{AB}$, so P_{WAB} must contain the cylinder axis. Next, line $\overline{AQ}$, is a chord of the circle that is a cross section of the cylinder. Therefore, the bisection line $\overline{MW}$ will intersect with the cylinder axis. However the cylinder axis is contained by plane P_{WAB}. Consequently, the intersection point, W, of line $\overline{MW}$ and plane P_{WAB} must be on the cylinder axis. Also, by definition, the distance between points W and A is the cylinder radius. $\qquad$ Q.E.D.

Notationally, the coordinates of point M are given by

$$(X_M, Y_M, Z_M) = \tfrac{1}{2}(X_A + X_Q, Y_A + Y_Q, Z_A + Z_Q)$$

and line direction of $\overline{MW}$, $\overrightarrow{U_{\overline{MW}}}$, can be expressed as

$$\overrightarrow{U_{\overline{MW}}} = \overrightarrow{U_{\overline{AB}}} \times \overrightarrow{U_{\overline{AQ}}} / |\overrightarrow{U_{\overline{AB}}} \times \overrightarrow{U_{\overline{AQ}}}|$$

where $\overrightarrow{U_{\overline{AQ}}} = (X_A - X_Q, Y_A, -Y_Q, Z_A - Z_Q)$. Thus the parametric form of line $\overline{MW}$ is given by

$$(X, Y, Z) = (X_M, Y_M, Z_M) + \beta(\overrightarrow{U_{\overline{MW}}})$$

where β is a scalar parameter. The normal vector of plane P_{WAB} is given by

$$\overrightarrow{U_{P_{WAB}}} = \overrightarrow{U_{\overline{AB}}} \times \overrightarrow{U_{BP_{\overline{AB}}}} / |\overrightarrow{U_{\overline{AB}}} \times \overrightarrow{U_{BP_{\overline{AB}}}}|$$

and the plane equation of P_{WAB} is expressed through a dot product

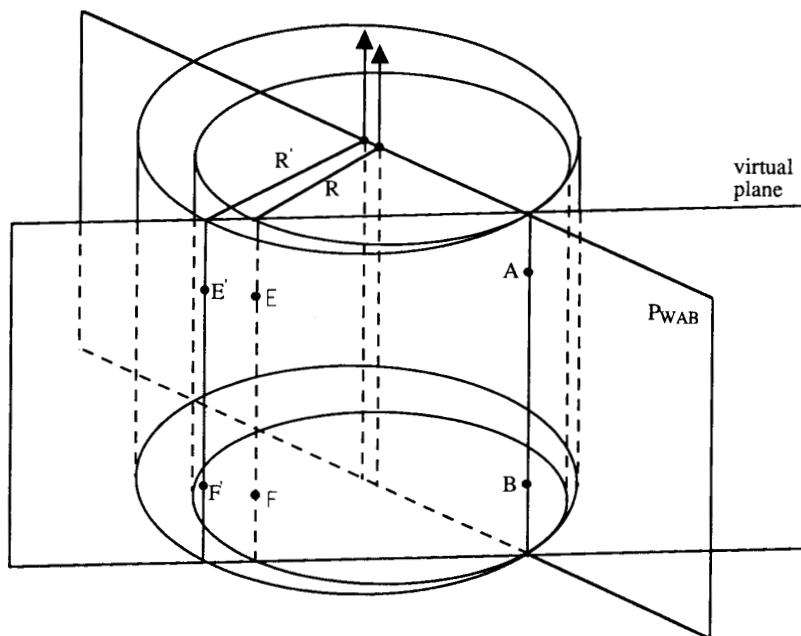$$\overrightarrow{U_{P_{WAB}}} \cdot (X - X_A, Y - Y_A, Z - Z_A) = 0.$$

Fig. 11.   The geometry for the estimation of the new cylinder radius and the new cylinder axis under the iterative measurement refinement procedure.

Finally, the parametric form of the cylinder axis can be expressed as

$$(X, Y, Z) = (X_W, Y_W, Z_W) + \gamma(\overrightarrow{U_{AB}})$$

where γ is a scalar parameter. Thus the location of the cylinder axis has been determined. Also the cylinder equation can be obtained from the given point W, cylinder axis direction, and cylinder radius.

V. THE ESTIMATION OF CYLINDER HEIGHT

When the rims of the top and bottom faces of a cylinder are within the field of view, then the cylinder height can be estimated; otherwise, it is too tall to be estimated from its image data. The basic idea is to find two image points u and v from the top and bottom rims of the cylinder image. Then the two rays constructed from these two image points to the vantage point, respectively, will intersect with the cylinder surface. The corresponding intersection points U and V on the top and bottom planar faces can be found. From these two points we can find the two plane equations of the top and bottom faces and then find the two intersection points of the two faces with the cylinder axis. Finally, we can compute the cylinder height as the distance between the two intersection points on the cylinder axis. The estimation procedure is described as follows.

A. Procedure for Estimation of Cylinder Height

1) From a vertical line profile of the cylinder image, find the two endpoints of the profile, called u and v. These two points correspond to two rim points on the top and bottom cylinder faces (as shown in Fig. 6(a)).

2) Construct two rays from the vantage point O_v to the two rim points u and v to obtain the two ray equations.
3) From the ray equations and the cylinder equation, find the 3-D coordinates of the corresponding points U and V on the cylinder top and bottom faces, respectively (see Fig. 6(b)). There will be two solutions to U or V. Choose the one according to a selection rule described below.
4) From points U and V, obtain the plane equations of the cylinder top and bottom faces. Find the intersections of the cylinder axis with these two faces, U_T and V_B.
5) Compute the distance between points U_T and V_B, $D_{\overline{U_T V_B}}$. This distance is the cylinder height.

The selection rule used in Step 3 is described here. Let θ_1 be the angle between the cylinder axis and the viewer viewing direction. Also let θ_2 be the angle between the cylinder axis and the light traveling direction. There are nine possible combinations of $\cos \theta_1$ and $\cos \theta_2$, as shown in Fig. 7. It can be shown that

1) If $\cos \theta_1 \cdot \cos \theta_2 \leq 0$, then the correct solution for point U or V is one of two solution points produced in Step 3 that is closer to the vantage point,
2) If $\cos \theta_1 \cdot \cos \theta_2 > 0$, and
   a) if the image point u or v used in Step 3 is on the rim of the planar face that is closer to the vantage point, then choose one of the two solution points that is farther from the vantage point.
   b) if the image point u or v used in Step 3 is on the planar face that is farther from the vantage point, then choose one of two solution points that is closer to the vantage point.
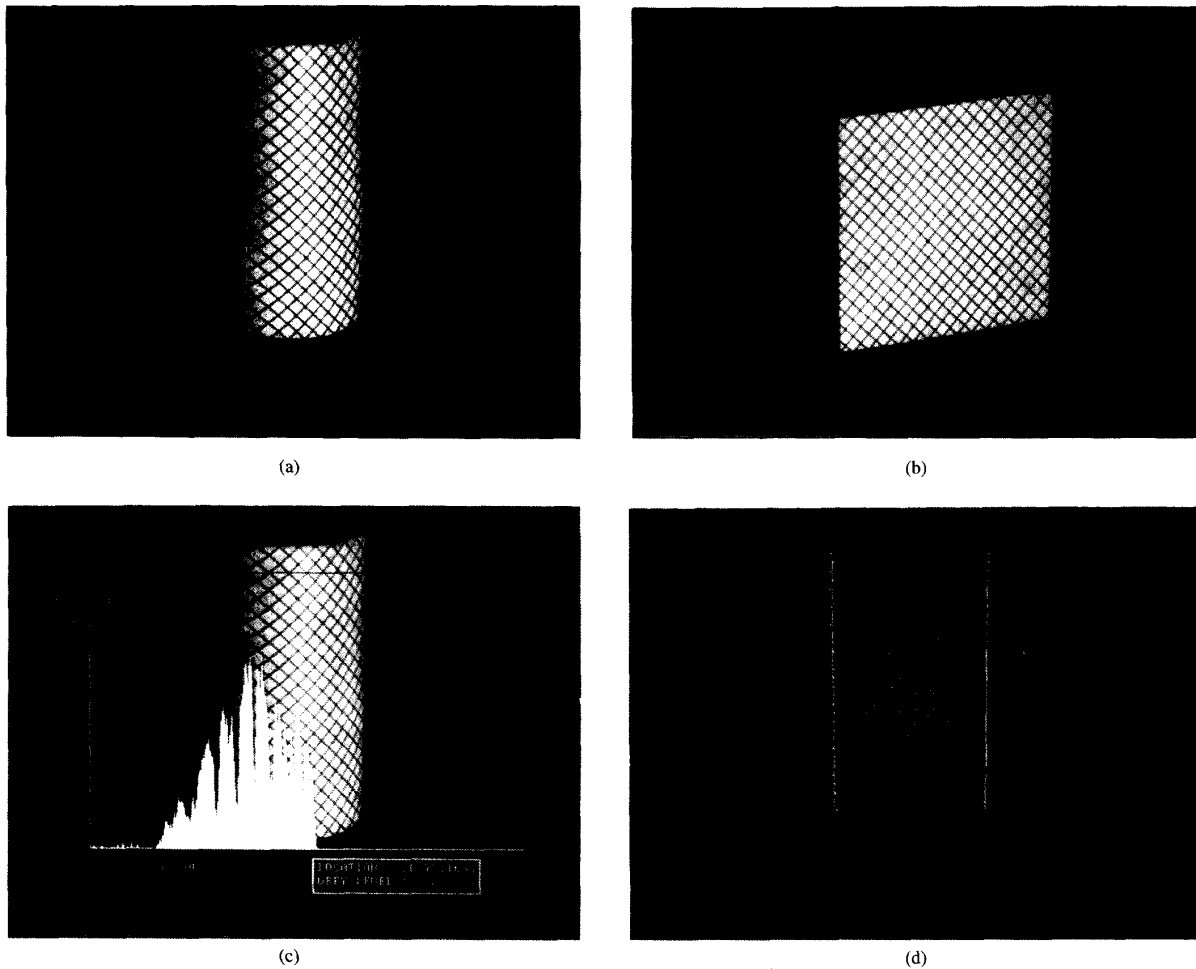
Fig. 12. The intermediate processing results of a grid-encoded cylinder. (a) A grid-encoded image. (b) The calibration plane image. (c) The row image profile of a scan line. (d) The perceived boundary points (+), the least-squared fitted silhouette edges, and the constructed grid pattern on the virtual plane.

The above selection rule is based on the fact the correct solution point must be on the visible rim that constitutes part of the object occluding boundary.

VI. EXPERIMENTS AND SENSITIVITY ANALYSIS

A. Experiment Description

Now we shall conduct real experiments to illustrate the actual implementation of the measurement (or estimation) method developed in the previous sections. The experiment apparatus consists of a structured light projector, a CCD camera and an IBM compatible PC [24]. The structured light projector consists of a gas laser, a laser beam expander, and an optical bench placed on an optical table. A cylindrical parallel light will be generated by the projector after a careful lens alignment. Then the cylindrical light beam passes perpendicularly through a grid plate marked with two sets of equally spaced, parallel lines that are orthogonal to each other. The illumination of these two sets of light sheets on an object creates a grid pattern on the object surface.

Let the cylinder to be measured be placed on the optical table in an upright position. We rotate the grid plate such that the two sets of light sheets intersect with the cylinder roughly diagonally. (The alignment is only rough; no precise alignment is required). Next, the camera geometry can be defined by its relative coordinates with respect to the optical table and the laser beam direction. In Fig. 8, a coordinate system is defined on the optical table whose Y_0 axis and Z_0 axis are along the laser beam direction and the normal vector of the table, respectively. The origin of the coordinate system is an arbitrary point on the table. Then the camera geometry can be defined by the location of the lens center and the optical axis with an orientation specified by the angle, called α, between the optical axis and the Z_0 axis and the angle, called θ, between the projected optical axis on the table and the Y_0 axis.

Before the actual measurement is conducted, the normal vectors of the two sets of light sheets $\overrightarrow{U_{LS_{12}}}$ and $\overrightarrow{U_{LS_{34}}}$ must be determined in the camera coordinate system by a calibration process [24] that will be briefly described below. In the calibration process an opaque planar calibration surface is
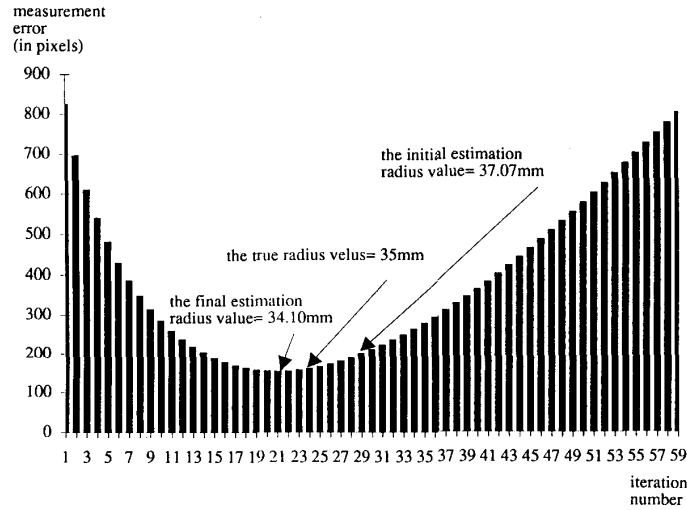
Fig. 13. The measurement error under the iterative measurement refinement procedure.

TABLE II
MEASUREMENT RESULTS OF THREE CYLINDERS WITH THE CONFIGURATION PARAMETERS
$\theta = 30°, \alpha = 100°$ AND $70°$, AND THE CAMERA-TO-OBJECT DISTANCE IS ABOUT 1000 MM

α	est. value items ╲ object	C1 (35 mm, 125 mm)	C2 (35 mm, 80 mm)	C3 (15 mm, 80 mm)
100°	Radius	36.29	36.49	15.84
	R. error %	3.69	4.26	5.60
	Height	123.91	75.87	77.16
	H. error %	0.87	5.16	3.55
70°	Radius	34.10	33.16	14.54
	R. error %	2.57	5.26	3.00
	Height	125.81	79.05	77.23
	H. error %	0.64	1.18	3.46

The average radius error % = 4.07%
The average height error % = 2.48%

placed on the laser beam path with a surface orientation that is perpendicular to the laser beam direction. Then a stripe pattern with equal-sided grids on the calibration plane is obtained. Through the grid coding analysis, the orientations of the grid lines that represent the normal vectors of the two sets of light sheets are computed. In the calibration method and the subsequent planar object surface measurement only the normal vectors of light sheets are needed—the actual identification of plane equations of the light sheets is not required—so this method is a correspondenceless method [24].

Next, we shall describe the estimation procedure used for the cylinder measurement that includes the image processing tasks for extracting the curved grid line pattern and the grid line endpoints in the image.

1) Construct the row image profile of each scan line in the image, as shown in Fig. 12(c). Check if the horizontal line image profile contains apparent (i.e., sharp) peaks and valleys. (Here the background is created by placing the cylinder against a black table cloth.) If yes, find the two endpoints of the profile that correspond to the two boundary points of the cylinder. Also, extract all valleys that correspond to grid points on each grid line.

2) From the endpoints of all scan lines, apply the least-squares line fitting to obtain the two perceived silhouette edges $\overline{ab}$ and $\overline{ef}$. (The silhouette edge $\overline{ab}$ with a high edge contrast corresponds to the tangent line on the cylinder surface drawn from the camera lens center, while the other edge $\overline{ef}$ with a smaller contrast, but
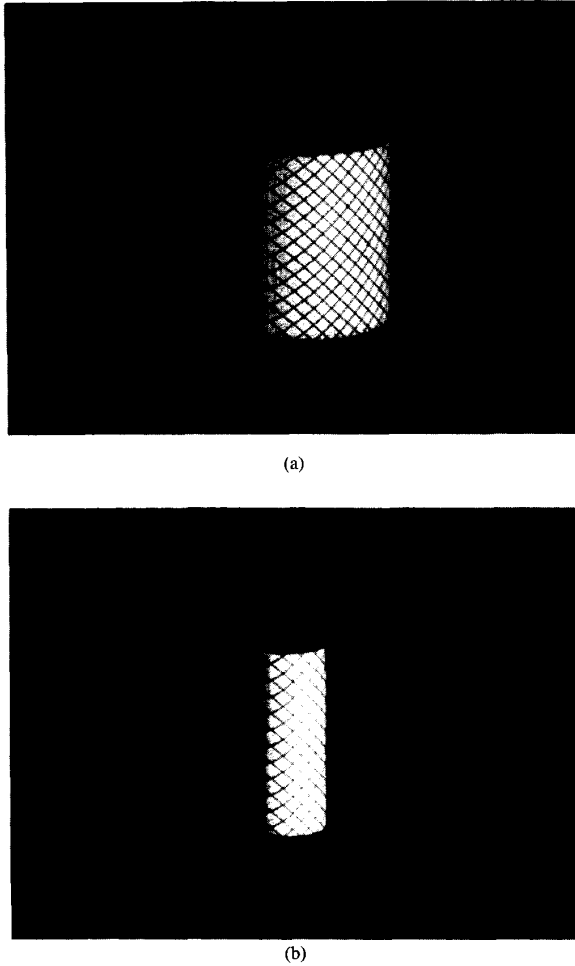
(a)

(b)

Fig. 14.   Two cylinders used in the experiments. (a) Cylinder C2 (radius = 35 mm, height = 80 mm). (b) Cylinder C3 (radius = 15 mm, height = 80 mm).

a steadily increasing gray intensity, corresponds to the tangent line created by the laser beam.)

3) (Construct the perceived curved grid lines and junctions) For each valley point on the current scan line, find if there is any single connected valley point on the next scan line. If yes, the two valley points are on the same grid line; if not, check whether there are any valley points within a prespecified neighborhood interval. In the case where there are two valley points (this is the case when a junction is nearby), choose the one along the local line direction of the grid line. In a case where there is no valley point indicates that the grid line is near the end or there is noise. Also find the junction where two grid lines merge.

4) (Find the intersection points of all perceived curved grid lines with the two perceived silhouette edges $\overline{ab}$ and $\overline{ef}$) Check the neighborhood of the endpoints of each perceived curved grid line to see if the grid line contains a point on the silhouette edge. If it does, find the intersection point directly or, if necessary, by an

extrapolation method based on the local line direction at the endpoint of the grid line; if it does not, this is an indication that the grid line intersects with the top or bottom faces of the cylinder, so the current grid line is not used.

5) (Find the grid pattern on the virtual plane in the image) Based on the intersection points of the perceived curved grid lines with the two perceived silhouette edges, construct the grid pattern on the virtual plane, as shown in Fig. 12(d).

6) Find the plane equation of the virtual plane in 3-D space using the technique presented in Section III.

7) Find the 3-D line equations of silhouette edges $\overline{AB}$ and $\overline{EF}$ on the virtual plane. The line direction of $\overline{AB}$ is the direction of the cylinder axis.

8) Based on $\overline{AB}$ and $\overline{EF}$, find the cylinder radius and a reference point on the cylinder axis using the developed technique given in Section IV.

9) Based on the sum of squares of distances between the estimated junctions and the actual junctions on the image plane, apply the iterative measurement refinement procedure (to be described later) to obtain the best estimation of the cylinder radius and a reference point on the cylinder axis.

10) Find the two endpoints on a vertical line profile of the cylinder image. They correspond to two rim points on the top and bottom faces of the cylinder image. Find the cylinder height based on these two rim points using the technique given in Section V.

B. Sensitivity Analysis

1) The Effect of Variations in the Endpoints of the Perceived Curved Grid Lines on the Virtual Plane Computation: The computation of the 3-D virtual plane is completely based on the grid lines on the perceived virtual plane constructed from the pairs of endpoints of the perceived curved grid lines, as shown in Fig. 12(d) and Fig. 9. Assume that the virtual plane grid line has length l and slope δ and its two endpoints have uncertainty quantities of ΔX and ΔY. Then the grid line has a new slope δ' after inclusion of $\Delta X, \Delta Y$ perturbations,

$$\tan \delta' = (\ell \sin \delta + \Delta Y)/(\ell \cos \delta + \Delta X).$$

If $\max(|l \sin \delta|, |l \cos \delta|) \gg \max\{|\Delta X|, |\Delta Y|\}$, then $\Delta \delta = \delta' - \delta$ is very small. In the experiments, $\delta \approx 45°, l \approx 200$ pixels, $|\Delta X| \leq 2$ pixels, and $|\Delta Y| \leq 2$ pixels. Therefore, the uncertainty of the two endpoints of the perceived curved grid lines has very small effect on the computation of the 3-D virtual plane equation. This will be confirmed by the experimental results of the endpoints noise analysis. (See Table I).

2) The Effect of the Positional Shift of the Perceived Silhouette Edges $\overline{ab}$ and $\overline{ef}$ on the Cylinder Measurement: The cylinder measurement depends on the positions of the perceived silhouette edge $\overline{ab}$ and $\overline{ef}$. From the optical nature of silhouette edge formation, it can be seen from the real image that $\overline{ab}$ is associated with a very sharp edge profile, while $\overline{ef}$ is with a small, but steadily varying edge profile (see Fig. 12(c)).

TABLE III
ORIENTATION ERROR OF THE VIRTUAL PLANE FOR DIFFERENT PERTURBATION OF THE ENDPOINTS OF STRIPE LINES BY SIMULATION (UNIT = DEGREE, STEP SIZE = 1 PIXEL)

ΔY \\ ΔX		2	4	6	8
2	mean	0.922	1.268	1.661	2.074
	S.D.	0.481	0.619	0.772	0.934
4	mean	1.417	1.601	1.999	2.269
	S.D.	0.728	0.823	1.013	1.131
6	mean	2.047	2.177	2.401	2.696
	S.D.	1.039	1.111	1.234	1.363
8	mean	2.691	2.833	2.967	3.199
	S.D.	1.361	1.456	1.516	1.644

S.D. = standard derivation

Therefore, the variation in edge $\overline{ab}$ is virtually zero and the variation in edge $\overline{ef}$ is roughly a translational shift, but the line orientation remain almost unchanged.

An iterative measurement refinement procedure can be developed to take the variation of the positional shift of silhouette edge $\overline{ef}$ into consideration. At the same time, the above procedure can also verify the goodness of the measurement results. In Fig. 10, let the grid pattern of the virtual plane image contain N points $g_i, i = 1, 2, \cdots, N$. For each of these N grid points we can draw a line from the camera lens center through g_i that intersects with the virtual plane in the space at G_i. The laser light ray passing G_i is given by parametric form:

$$\begin{bmatrix} X \\ Y \\ Z \end{bmatrix} = (\overrightarrow{U_{\text{LS}_{12}}} \times \overrightarrow{U_{\text{LS}_{34}}})^t \cdot t_J + \begin{bmatrix} X_{G_i} \\ Y_{G_i} \\ Z_{G_i} \end{bmatrix}.$$

There are two intersection points between the above light ray and the estimated cylinder. Choose the one with a negative value of t_{J_i} to be the junction J_i on the curved cylinder surface visible to the camera. Use the perspective projection of junction J_i to find the projected junction j'_i on the image plane. Assume the coordinates of the actual perceived junction (identified by the two associated perceived curved grid lines) are given by $(j_x, j_y)_i$. We then define a measurement error as

$$\text{Measurement error} = \sum_{i=1}^{N} [(j_x - j'_x)_i^2 + (j_y - j'_y)_i^2]^{1/2}.$$

The iterative measurement refinement procedure is given as follows. Refer to Fig. 5.

1) Let point Q be shifted along the line $\overline{AM}$ by a step size = 0.02 * initial radius value to either side of the original position in a fixed number of iterations.
2) Apply the measurement technique to find the new cylinder radius and the new cylinder axis, as shown in Fig. 11.
3) Use the new cylinder radius and the new cylinder axis obtained in the current iteration to compute the estimated junctions on the cylinder surface and compute the measurement error for the current iteration.
4) After the computations of measurement errors for all iterations are obtained, as shown in Fig. 13, find the one with the minimum error. This result is our final solution.

C. A Typical Experimental Result

Now we shall give the intermediate processing results of a typical experiment. The cylinder used is identified as C1 with radius = 35 mm and height = 125 mm. The grid-encoded image shown in Fig. 12(a) is taken. The grid plate used has a 5 mm grid size, the camera focal length is 25 mm, the image X, Y aspect ratio is $1 : 1.229$. The calibration plane image shown in Fig. 12(b) is analyzed to produce the following results.

1) The plane equation of the calibration plane is $-0.402x + 0.319y + 0.859z = 841.37$.
2) The normal vectors of the two sets of light sheets are $\overrightarrow{U_{\text{LS}_{12}}} = (0.668, -0.540, 0.513)$ and $\overrightarrow{U_{\text{LS}_{34}}} = (0.627, 0.780, 0.004)$.

The typical row image profile of a scan line is given in Fig. 12(c). The perceived boundary points, the least-squared fitted silhouette edges and the constructed grid pattern on the virtual plane are shown in Fig. 12(d). The 3-D virtual plane equation is found to be $-0.262x + 0.001y + 0.965z = 1021.17$.

The 3-D silhouette edges are $\overline{AB}$ = (0.022, 0.999, 0.006), $\overline{EF}$ = (0.007, −0.999, 0.002). The initial values of feature points shown in Fig. 5 are found to be

1) A = (26.97, 51.08, 1065.60);
2) Q = (−41.57, 52.69, 1046.96);
3) M = (−7.30, 51.88, 1056.28);
4) W = (−10.08, 51.88, 1066.50); and
5) radius = 37.07.

After the iterative measurement refinement procedure shown in Fig. 13, the final radius is 34.10 mm. (The true radius value = 35 mm.) In the computation of the cylinder height, the two rim points used are u = (2.08, 75.16, 1033.59) and v = (2.08, −50.68, 1033.69). The cylinder height is 125.81 mm. (The true height is 125 mm.)

D. Experiment Results with a Wide Range of Geometric Configuration Parameters for Three Different Cylinders

Three different cylinders, identified as C1, C2, and C3, are used. They have a combination of radius and height of (35 mm, 125 mm), (35 mm, 80 mm), and (15 mm, 80 mm), respectively. The grid-encoded images of the cylinders C2 and C3 are given in Figs. 14(a) and 14(b). Table I gives the measurement results of the three cylinders for the first set of geometric configuration parameters where $\alpha = 90°, \theta = 15°, 30°$, and $45°$ and the camera-to-object distance is about 900 mm, where α and θ are defined in Fig. 8. From this table we can see that the average radius error = 4.16% and the average height error = 3.5%. Table II gives the measurement results of three cylinders with the configuration parameters $\theta = 30°, \alpha = 100°$ and $70°$. The average radius error is 4.07%, and the average height error is 2.48%. From these two tables our cylinder measurement method is quite successful and stable.

E. The Stripe Endpoint Noise Analysis

To study the sensitivity or stability of the cylinder estimation technique in the presence of noise in the endpoints of the perceived curved grid lines, we also conduct a stripe endpoint noise analysis using an error model shown in Fig. 9. The orientation error associated with $|\Delta X|$ and $|\Delta Y|$ variations is defined as the absolute difference of the virtual plane orientation angles with and without $|\Delta X|$ and $|\Delta Y|$ variations. The orientation errors of the virtual plane incurred are shown in Table III. From the table it can be seen that the mean of the error is less than $3.2°$ and the S.D. is less than $1.6°$. Therefore, the 3-D virtual plane computation is quite stable in the presence of noise.

VII. CONCLUDING REMARKS

We have presented a complete method for estimating the cylinder axis orientation and location, radius, and height of a cylinder. The method used is a spatial encoding technique. A crucial step in this study is to convert the complicated curved stripe estimation problem to a simpler line stripe estimation problem. Then we use the observable or constructible geometric entities to estimate the location and shape parameters of the cylinder. To confirm the developed theory for cylinder mea-

surement, an experiment apparatus has been set up to actually estimate the cylinder shape parameters from a single image for three different cylinders under a variety of measurement environments. An iterative measurement refinement procedure for minimizing an error measure is shown to be able to yield good measurement results. The sensitivity analysis of effect of stripe endpoint uncertainty on the estimation indicates that the method is quite stable. At present, we are investigating the method for automatic determination of the correct geometric configuration of laser projector, camera, and object so that a cylinder from a family of cylinders with known radius and height ranges can be measured in a configuration automatically set up without human intervention.

REFERENCES

[1] S. M. Bhandarhar and M. Suk, "Recognition and localization of objects with curved surface," *Machine Vision and Application*, no. 4, pp. 15–31, 1991.
[2] S. M. Dunn, R. L. Keizer, and J. Wu, "Measuring the area and volume of the human body with structured light," *IEEE Trans. Syst. Man Cyber.*, vol. 19, no. 6, pp. 1350–1364, 1989.
[3] N. J. Foster and A. C. Sanderson, "Determining object orientation using ellipse fitting," *Proc. of SPIE*, vol. 521, pp. 34–43, 1984.
[4] Y. C. Shiu and S. Ahmad, "3D location of circular and spherical features by monocular model-based vision," in *Proc. 1989 IEEE Int. Conf. Syst. Man, Cyber.*, Nov. 1989, pp. 576–581.
[5] R. M. Bolle and B. C. Vemuri, "On three-dimensional surface reconstruction methods," *IEEE Trans. Pattern Anal. Machine Intell.*, vol. 13, no. 1, pp. 1–13, 1991.
[6] G. J. Agin and T. O. Binford, "Computer description of curved objects," *IEEE Trans. Comput.*, vol. 25, no. 4, pp. 439–449, 1976.
[7] R. J. Popplestone, C. M. Brown, A. P. Ambler, and G. F. Crawford, "Forming models of plane-and-cylinder faceted bodies from light stripes," in *Proc. 4th Int. Joint Conf. Artificial Intelligence*, 1975, pp. 664–668.
[8] B. Cernuschi-Frias and D. B. Cooper, "3-D space location and orientation parameter estimation of Lambertian spheres and cylinders from a single 2-D image by fitting lines and ellipses to thresholded data," *IEEE Trans. Pattern Anal. Machine Intell.*, vol. 6, no. 4, pp. 430–441, 1984.
[9] A. Jarvis, "A perspective on range finding techniques for computer vision," *IEEE Trans. Pattern Anal. Machine Intell.*, vol. 11, no. 4, pp. 460–471, 1989.
[10] D. B. Gennery, "Object detection and measurement using stereo vision," in *Proc. 6th Int. Joint Conf. Artificial Intelligence*, 1979, pp. 320–327.
[11] M. C. Chiang and J. B. K. Tio, "Robot vision using a projection method," *Proc. SPIE*, vol. 449, pp. 74–81, 1983.
[12] T. Lozano-Perez, W. E. L. Grimson, and S. J. White, "Finding cylinders in range data," in *Proc. 1987 IEEE Int. Conf. Robotics Automat.*, 1987, pp. 202–207.
[13] D. G. Lowe, "Three-dimensional object recognition from single two-dimensional images," *Artificial Intelligence*, vol. 31, pp. 355–395, 1987.
[14] Y. F. Wang and J. K. Aggarwal, "Integration of active and passive sensing techniques for representing three-dimensional objects," *IEEE Trans. Pattern Anal. Machine Intell.*, vol. 11, no. 4, pp. 460–471, 1989.
[15] A. Asada, H. Ichikawa, and S. Isuji, "Determining surface orientation by projecting a stripe pattern," *IEEE Trans. Pattern Anal. Machine Intell.*, vol. 10, no. 5, pp. 749–754, 1988.
[16] N. Shrikhande and G. Stockman, "Surface orientation from a projected grid," *IEEE Trans. Pattern Anal. Machine Intell.*, vol. 11, no. 6, pp. 650–655, 1989.
[17] Y. F. Wang, A. Mitiche, and J. K. Aggarwal, "Computation of surface orientation and structure of objects using grid coding," *IEEE Trans. Pattern Anal. Machine Intell.*, vol. 9, no. 1, pp. 129–137, 1987.
[18] Y. F. Wang, "Characterizing 3D surface structured from visual images," *IEEE Trans. Pattern Anal. Machine Intell.*, vol. 13, no. 1, pp. 51–60, 1991.
[19] P. Vuylsteke and A. Oosterlinck, "Range image acquisition with a single binary-encoded light pattern," *IEEE Trans. Pattern Anal. Machine Intell.*, vol. 12, no. 2, pp. 148–164, 1990.
[20] P. M. Will and K. S. Pennington, "Grid coding: a novel technique for image processing," *Proc. IEEE*, vol. 60, no. 6, pp. 669–680, 1972.

[21] G. Hu and G. Stockman, "3-D surface solution using structured light and constraint propagation," *IEEE Trans. Pattern Anal. Machine Intell.*, vol. 11. no. 4, pp. 390–402, 1989.

[22] E. L. Hall, J. B. K. Tio, C. A. McPherson, and F. A. Sadjadi, "Measuring curved surfaces for robot vision," *Computer*, vol. 15, no. 12, pp. 42–54, 1982.

[23] P. R. Hangen, R. E. Keil, and C. Bocchi, "3-D active vision system," *Proc. SPIE*, vol. 521, pp. 258–263, 1984.

[24] D. C. Tseng and Z. Chen, "Computing location and orientation of polyhedral surface using a laser-based vision system," *IEEE Trans. Robotics Automat.*, vol. 7, no. 6, pp. 842–848, 1991.

Tsorng-Lin Chia was born in Peng-Hu, Taiwan, R.O.C., in 1961. He received the B.S. degree in electrical engineering from Chung Cheng Institute of Technology, Taoyuan, Taiwan, in 1982, and the M.S. degree in computer engineering from National Chiao-Tung University, Hsinchu, Taiwan, in 1986. He is presently working toward the Ph.D. degree in the Institute of Computer Science and Information Engineering at National Chiao-Tung University, Hsinchu, Taiwan. During 1986–1989, he was a lecturer with the Department of Electrical Engineering at Chung Cheng Institute of Technology. His research interests include image processing, pattern recognition, computer vision, and parallel algorithm and architecture.

Zen Chen received the B.Sc. degree from National Taiwan University, Taiwan, R.O.C., in 1967, the M.Sc. degree from Duke University, Durham, NC, in 1970, and the Ph.D. degree from Purdue University, West Lafayette, IN, in 1973, all in electrical engineering.

After graduating from Purdue University, he joined Burroughs Corporation, Detroit, MI, where he was engaged in the development of document recognition system. He has been on the faculty of National Chiao Tung University, Taiwan, R.O.C. since 1974, where he is currently a Professor of computer science and information engineering. He served as Director of the Institute of Computer Engineering from 1975 to 1980 and 1989 to 1991. He spent the academic year 1981–1982 at Lawrence Berkeley Laboratory, University of California, Berkeley, CA, as a visiting scientist. During 1989–1990, he spent six months at the Center for Automation Research, University of Maryland, College Park, MD, as a visiting professor. His current research interests include computer vision, pattern recognition, CAD/CAM, expert system, and parallel algorithm and architecture. He has consulted for various government agencies and industrial organizations in these areas.

Dr. Chen is a member of Sigma Xi, Phi Kappa Phi, China Computer Society and the Chinese Institute of Electrical Engineering. He served as the first President of the Chinese Image Processing and Pattern Recognition Society during 1990–1992.

Shinn-Ying Ho was born in Taiwan, R.O.C., on March 25, 1962. He received the B.S., M.S., and Ph.D. degrees in computer science and information engineering from National Chiao Tung University, Hsinchu, Taiwan, in 1984, 1986, and 1992, respectively. He is currently an associate professor in the Department of Information Engineering at Feng-Chia University, Taichung, Taiwan. His research interests include image processing, pattern recognition, and applications of computer vision in robotics and automation.